


Two-Stage Guidance Law With Constrained Impact via Circle Involute

ZIQI WANG 
QINGLEI HU , Senior Member, IEEE
TUO HAN 
Beihang University Beijing, China

MING XIN , Senior Member, IEEE
University of Missouri, Columbia, MO, USA

The mission of simultaneous attack and warhead lethality enhancement requires the constraints on impact time and angle in the guidance design. To this end, a two-stage guidance law considering constrained impact as well as the robustness against external disturbances and heading errors is proposed. The first stage is based on a circle involute geometrical rule that guarantees the desired velocity direction at the involute's end. With this goal achieved, the involute guidance is switched to the guidance of nullifying line-of-sight rate such that near-zero maneuver in the second stage is ensured. To achieve both impact time and angle constraints, a simple parameter determination approach is provided to find explicit solutions for the desired two-stage trajectory. Meanwhile, a robust two-stage guidance law is constructed to implement the geometrical rule, guarantee terminal constraints, and ensure robustness. The proposed technique is easy to implement, in that it does not involve model linearization, time-to-go estimation, and numerical optimization routine. Additionally, the achievable range of different constraints is analyzed considering practical issues such as initial launch angles, initial line-of-sight angles, and acceleration limits. Extensive simulations are carried out in various engagement scenarios under uncertainties and disturbances to validate the effectiveness and robustness of the proposed guidance law.

Manuscript received March 4, 2020; revised September 2, 2020 and November 1, 2020; released for publication November 9, 2020. Date of publication November 25, 2020; date of current version April 10, 2021.

DOI: No. 10.1109/TAES.2020.3040524

Refereeing of this contribution was handled by S. Le Menec.

This work was supported in part by the National Natural Science Foundation of China under Grant 61960206011 and Grant 61633003, and in part by the Beijing Natural Science Foundation under Grant JQ19017.

Authors' addresses: Ziqi Wang, Qinglei Hu, and Tuo Han are with the School of Automation Science and Electrical Engineering, Beihang University, Beijing 100191, China, E-mail: (ziqu_wang@buaa.edu.cn; huql_buaa@buaa.edu.cn; hantuo@buaa.edu.cn); Ming Xin is with the Department of Mechanical and Aerospace Engineering, University of Missouri, Columbia, MO 65211 USA, E-mail: (xin@missouri.edu). (*Corresponding author: Qinglei Hu.*)

0018-9251 © 2020 IEEE

I. INTRODUCTION

The recently developed advanced guidance laws aim to intercept the target at a specified impact angle or impact time for better interception effectiveness. For example, a specified impact angle can improve missile survivability by escaping the directional defense zone, and a specified impact time can be used to conduct a salvo attack. However, aspects such as feasibility, robustness, and implementation complexity of the constrained guidance laws are currently significant issues that attract the considerable interest of research.

As for the impact angle guidance (IAG) laws, one of the earliest works was done by Kim and Grider [1]. They proposed a terminal guidance law for reentry vehicles with an impact angle constraint by posing a linear-quadratic optimal control problem with time-varying feedback gains. Then, in [2], an IAG law based on linearized engagement models was designed through the optimal control method. Another group of IAG solutions is based on pure pursuit guidance and proportional navigation guidance (PNG). An adaptive PNG law was proposed in [3], where the navigation gain is updated by closed-loop nonlinear adaptation laws to achieve hypervelocity impact in a specified direction. A two-phase PNG law that satisfies an impact angle constraint was proposed in [4], where the required proportional navigation gain is solved numerically. In [5], an IAG law was proposed in a feedback form in terms of the instantaneous zero-effort-miss and intercept angle error with a time-varying navigation gain. Sliding mode control (SMC) was employed to IAG law in [6] to stabilize the designed line-of-sight (LOS) error dynamics. In [7], a cubic spline IAG law with two degrees of freedom was derived using the inverse method, and the capturability analysis of the guidance law was presented as a set of feasible boundary conditions. Meanwhile, IAG was investigated based on unique properties of the geometric curves, such as the circular curves used in [8]–[10], elliptic curves used in [11], and spirals like circle involutes and Archimedean spirals used in [12] and [13], respectively. It is worth noting that these geometric methods make the design of constrained guidance laws simpler and their implementations more feasible.

Another constraint that has been extensively studied is the impact time constraint. An early example of impact time guidance (ITG) law was proposed in [14], where the prescribed impact time is achieved by introducing feedback of the impact time error to the PNG law. Besides, the ITG laws were also derived through SMC [15] and Lyapunov-based control [16]. In [17], a differential geometric guidance approach was presented by using the involute of the target's curve to meet the desired impact time. Tsalik and Shima [18] proposed a circular-based guidance law to impose a specified impact time by constraining the interceptor to travel along a circular trajectory towards the target. To not depend on the precise estimation of time-to-go, Tekin *et al.* used polynomial shaping of the look angle to solve the ITG problem against a stationary target considering constant and varying missile velocities, respectively in [19], [20]. In [21], instead of shaping the look angle, the authors formulated

the range to target as a general-order polynomial in time to satisfy an impact time constraint. In [22], a two-stage guidance scheme consisting of decentralized control law and a pure PNG law was proposed to achieve a salvo-attack against a stationary target. More recently, a circular predictive guidance law utilizing a dual-virtual-target concept was developed in [23] to meet an impact time constraint.

Given the effectiveness of both the impact time and impact angle constraints, the guidance laws considering these two constraints simultaneously have attracted more attention in recent years. One of the main categorizations of the existing impact time and angle guidance (ITAG) approaches depends on whether a switching logic is employed or not. In the non-switching category, the first non-switching ITAG law was derived in [24] through optimal control theory, which consists of a feedback loop to achieve the desired impact angle and an additional control command to control the impact time. By using differential game theory, Kang and Kim [25] proposed an ITAG law that combines the optimal guidance to control the impact angle and an additional command to control the impact time. In [26], the ITAG problem is reduced to a two-point boundary value problem and solved by the shooting method. Kim *et al.* [27] introduced an ITAG law against stationary targets based on a polynomial function of the downrange-to-go with three unknown coefficients. The ellipse-based guidance law proposed in [28] can also impose the desired impact time and angle simultaneously. In the switching category, the ITAG strategies consist of at least two guidance laws and a corresponding switching logic. An early design of the switching ITAG strategy was developed in [29], where an IAG law using backstepping control and an ITG law based on PNG are combined to improve the kill probability. In [30], the impact angle and time constraints were satisfied by switching between an optimal control-based IAG law and an SMC-based ITG law. A hybrid guidance scheme comprising three guidance modes (the first mode with an impact angle constraint and the other two with an impact time constraint) was proposed in [31], where the switching logic is determined by the impact time error and range rate. In [32], a three-phase ITAG strategy was presented under the look-angle and acceleration constraints through an optimal control framework. More recently, Hu *et al.* [33] proposed an ITAG strategy based on the virtual target concept by combining an SMC-based IAG law and a PNG law.

Despite the recent progress in the aforementioned ITAG laws, the problem of ITAG law design remains open. For instance, the linearized kinematic model is employed in [24], [25], and [27], the error-prone estimation of time-to-go is demanded *a priori* in [24], [25], and [29]–[31], and the guidance parameters are tuned through time-consuming numerical optimization routines in [26], [32], and [33]. It is worth mentioning that these drawbacks can be avoided using geometric principles that guide the missiles to travel along specified curves [8]–[13], [17], [18], [23], [28]. In addition to such an advantage, the geometric guidance law is simple for implementation since the desired trajectory can be acquired explicitly in advance. However, most of

the geometric guidance laws only considered either impact angle constraint [8]–[13] or impact time constraint [17], [18], [23]. One work that considered both is the elliptic guidance (EG) [28], where the guidance law is derived by linearizing the missile's equations of motion around the elliptical trajectories.

Taking all the above issues into account, this work attempts to handle these challenges by designing a two-stage ITAG law based on the geometric property of the circle involute. Note that employing involutes in the guidance law design can be found in [12] and [17]. However, the geometrical rule was not given in [12], and the guidance law to maintain the missile along the involute was not shown in [17]. Moreover, neither of them meets both impact time and angle constraints. Compared to the existing ITAG law designs in the literature, the main contributions of the proposed ITAG law are presented as follows.

- 1) A circle involute-based two-stage guidance law that achieves the desired impact time and angle is designed, which does not involve model linearization, time-to-go estimation, numerical optimization routine, and complicated parameter calculations.
- 2) The robustness of the guidance law against external disturbances and heading errors is ensured via providing a geometrical rule and forcing it in the first stage while eliminating the LOS rate in the second stage.
- 3) The achievable range of different constraints is analyzed considering practical issues such as initial launch angles, initial LOS angles, and acceleration limits.

The rest of the article is organized as follows. In Section II, the planar engagement geometry and nonlinear kinematics against a stationary target are presented. Section III introduces the circle involute-based geometrical rule. The approach of finding the desired trajectories that meet different constraints, as well as feasibility analysis, is elaborated in Section IV. The guidance law that maintains the missile along the designed trajectory is derived in Section V. In Section VI, the effectiveness and robustness of the guidance law are validated by extensive simulations. Finally, Section VII concludes this article.

II. PROBLEM DESCRIPTION

A planar interception problem against a stationary target is considered. As shown in Fig. 1, the missile M is launched from the launch point L with a launch angle γ_L and travels along the trajectory toward a stationary target T with the desired impact angle γ_T . With respect to a horizontal reference, all the angles used in this article are defined as positive in the counterclockwise direction.

The missile is assumed to be moving at a constant speed V_M with its acceleration A_M perpendicular to the velocity vector. (x_M, y_M) and γ represent the position coordinate and the flight-path angle of the missile, respectively. The relative range and LOS angle between the missile and the

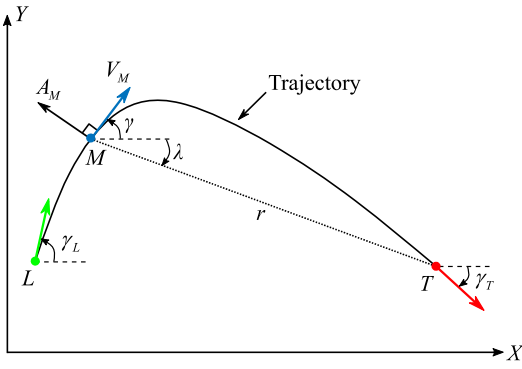


Fig. 1. Planar engagement geometry.

target are denoted as r and λ , respectively. In the inertial Cartesian frame, the nonlinear kinematic equations of the missile are given as

$$\begin{cases} \dot{x}_M = V_M \cos \gamma \\ \dot{y}_M = V_M \sin \gamma \\ \dot{\gamma} = \frac{A_M}{V_M} \end{cases} \quad (1)$$

The equations of missile-target relative motion in polar coordinates are described by

$$\begin{cases} \dot{r} = -V_M \cos(\gamma - \lambda) \\ r\dot{\lambda} = -V_M \sin(\gamma - \lambda) \end{cases} \quad (2)$$

In this article, the guidance mission with impact time and angle constraints can be described as the following objectives

$$\begin{cases} r_f \rightarrow 0 \\ t_f \rightarrow t_{\text{des}} \\ \gamma_f \rightarrow \gamma_T \end{cases} \quad (3)$$

where r_f , t_f , and γ_f denote the miss distance, final impact time, and final impact angle, respectively. t_{des} represents the desired impact time.

III. NEW GEOMETRICAL RULE BASED ON INVOLUTE OF A CIRCLE

In this section, the definition and unique properties of the involute of a circle are presented first. Then, the parametric equations for an involute trajectory with a specified impact angle are derived, followed by the geometrical rule to achieve such an involute trajectory.

A. Involute of a Circle

The geometric sketch of the involute of a circle is shown in Fig. 2. The center of the base circle is at origin O of the $X - O - Y$ Cartesian frame, and the radius of the circle is a . Then, the parametric equation [34] for the involute of a circle in the Cartesian frame is

$$\begin{cases} x = a(\cos \varphi + \varphi \sin \varphi) \\ y = a(\sin \varphi - \varphi \cos \varphi) \end{cases} \quad (4)$$

where φ is the angular parameter that indicates the position of point (x, y) on the involute, and it is defined as positive

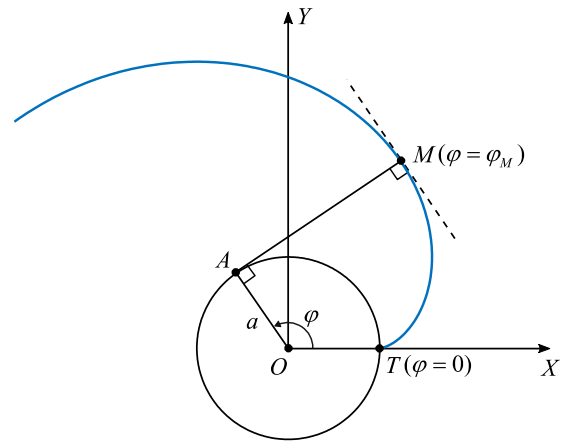


Fig. 2. Involute of a circle.

in the counterclockwise direction. For brevity, the word “involute” used in the following contents refers specifically to the involute of a circle.

The main mathematical/geometrical properties of the involute [34] that motivate the design of the guidance strategy in this work are illustrated in Fig. 2. First, the involute is tangent to the horizontal axis OX at its end ($\varphi = 0$), in this case at point T , and this property can be utilized to impose a specified impact angle. Second, the normal line to the involute at any point is tangent to the circle, which in this case, means that $MA \perp OA$. Third, the distance between any point M on the involute and its corresponding tangent point on the circle is equal to the length of a circular arc measured from $\varphi = 0$ to $\varphi = \varphi_M$, which means that $MA = \widehat{TA} = a\varphi_M$. The above properties are helpful in both trajectory planning and guidance law design.

B. Geometrical Rule

The new geometrical rule is to guide the missile along the involute of a circle toward the target, and different impact angles can be achieved by rotating the involute around the center of the circle. In this subsection, the parametric equations for the rotated involute and the geometrical rule to achieve such an involute trajectory are introduced.

As shown in Fig. 3, the coordinate of the center of the base circle in the $X - O - Y$ Cartesian frame is denoted as $O'(x_{O'}, y_{O'})$. To meet any desired impact angle, the involute can be rotated around O' by a corresponding angle θ , and the parametric equations for the rotated involute become

$$\begin{cases} x = x_{O'} + a(\cos(\varphi + \theta) + \varphi \sin(\varphi + \theta)) \\ y = y_{O'} + a(\sin(\varphi + \theta) - \varphi \cos(\varphi + \theta)) \end{cases} \quad (5)$$

For an impact angle between $[-\pi, \pi]$, the corresponding rotation angle can be obtained as $\theta = \gamma_T + \pi$. By substituting the expression of θ into (5), the parametric equations for an involute trajectory with an impact angle γ_T are given as

$$\begin{cases} x = x_{O'} - a(\cos(\varphi + \gamma_T) + \varphi \sin(\varphi + \gamma_T)) \\ y = y_{O'} - a(\sin(\varphi + \gamma_T) - \varphi \cos(\varphi + \gamma_T)) \end{cases} \quad (6)$$

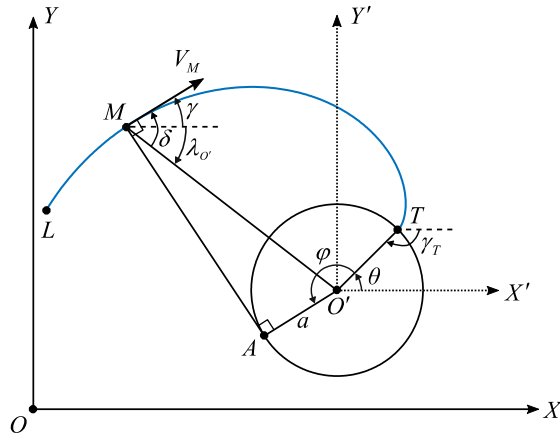


Fig. 3. Illustration of the geometrical rule.

Then, a geometrical rule is derived to achieve an involute trajectory defined by (6). As shown in Fig. 3, δ is the angle between the missile's velocity vector and the LOS between the missile and the center of the circle. Since the normal to a random point M on the involute is tangent to the circle at A , the missile's velocity vector is parallel to $O'A$. Therefore, δ and $\angle MO'A$ form a pair of alternate interior angles, which means that $\delta = \angle MO'A$. In the $\triangle MO'A$, the tangent of $\angle MO'A$ can be obtained as

$$\tan \delta = \tan \angle MO'A = MA/O'A = a\varphi/a = \varphi. \quad (7)$$

Since the normal to the involute is always tangent to the circle, angle φ is equal to the angle turned by the velocity vector from the missile's current position to the target, which yields

$$\varphi = \gamma - \gamma_T. \quad (8)$$

Finally, the geometrical rule for an involute trajectory with an impact angle γ_T can be written as

$$\tan \delta = \gamma - \gamma_T. \quad (9)$$

Note that δ can be obtained as $\delta = \gamma - \lambda_{O'}$, where $\lambda_{O'}$ can be calculated as

$$\lambda_{O'} = \tan^{-1} \frac{y_{O'} - y}{x_{O'} - x}. \quad (10)$$

Therefore, the center of the circle needs to be determined in advance to implement the geometrical rule in (9).

IV. TRAJECTORY DESIGN

To find the feasible trajectory based on the involute of a circle, the general approach for an impact angle constraint is presented first. By adding a straight segment, an improved two-stage approach is proposed to meet both impact and launch angle constraints. Then, the approach to find a trajectory that satisfies both impact time and impact angle constraints is described. Finally, analyses of feasible ranges of different constraints for both one-stage and two-stage trajectories are presented.

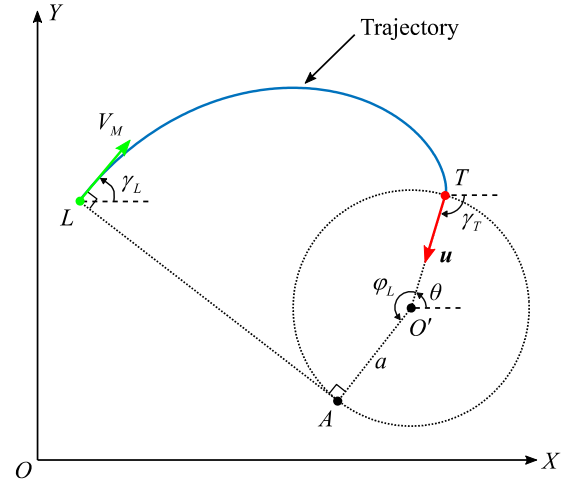


Fig. 4. Geometry of the pure involute trajectory.

A. General Approach for Impact Angle Constraint

In this subsection, the procedure of finding the involute trajectory with an impact angle constraint is presented. The geometry of the involute trajectory is shown in Fig. 4. The launcher $L(x_L, y_L)$ is assumed to be on the involute, and the target $T(x_T, y_T)$ is assumed to be at the involute's end. γ_L and γ_T represent the launch angle and impact angle, respectively. The unit vector of the final velocity vector of the missile is denoted as \mathbf{u} , and given as $\mathbf{u} = (\cos \gamma_T, \sin \gamma_T)$.

At the interception point T , the missile's final velocity vector \mathbf{u} points toward the center of the circle, which leads to

$$\mathbf{O}' = \mathbf{T} + a\mathbf{u} = (x_T + a \cos \gamma_T, y_T + a \sin \gamma_T). \quad (11)$$

By substituting (11) in (6), the parametric equations for the involute become

$$\begin{cases} x = x_T + a \cos \gamma_T - a(\cos(\varphi + \gamma_T) + \varphi \sin(\varphi + \gamma_T)) \\ y = y_T + a \sin \gamma_T - a(\sin(\varphi + \gamma_T) - \varphi \cos(\varphi + \gamma_T)) \end{cases} \quad (12)$$

Note that when $\varphi = \varphi_L$, launcher $L(x_L, y_L)$ is on the involute. Substituting $\varphi_L = \gamma_L - \gamma_T$ and $(x, y) = (x_L, y_L)$ into (12) yields

$$\begin{cases} x_L = x_T + a \cos \gamma_T - a \cos \gamma_L - a(\gamma_L - \gamma_T) \sin \gamma_L \\ y_L = y_T + a \sin \gamma_T - a \sin \gamma_L + a(\gamma_L - \gamma_T) \cos \gamma_L \end{cases} \quad (13)$$

Eliminating the variable a in (13) yields

$$\begin{aligned} (x_L - x_T)(\sin \gamma_T - \sin \gamma_L + (\gamma_L - \gamma_T) \cos \gamma_L) \\ - (y_L - y_T)(\cos \gamma_T - \cos \gamma_L - (\gamma_L - \gamma_T) \sin \gamma_L) = 0. \end{aligned} \quad (14)$$

Therefore, for a given engagement scenario, γ_L is dependent on the value chosen for γ_T and vice versa. This means that the involute trajectory that connects the launcher and target cannot satisfy a random combination of γ_L and γ_T . For a specified γ_T , solving the transcendental (14) numerically (like Newton's method or other numerical routines in [35] and [36]) yields the corresponding γ_L . Such calculation is easy to perform with fast determination because only

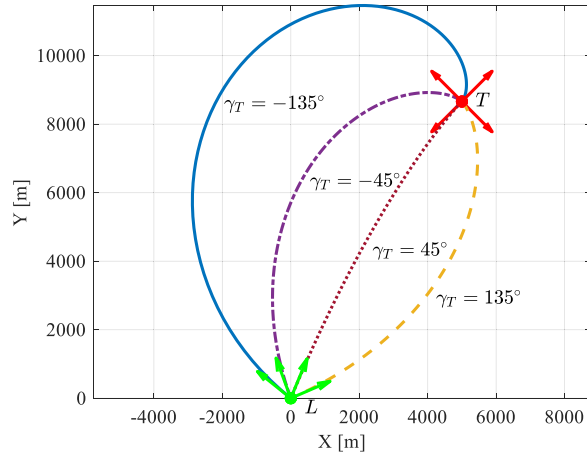


Fig. 5. Involute trajectories with different impact angles.

one single variable needs to be solved in (14). Moreover, it is worth noting that this process can be done offline before launch, thus it will not cause computation issues for implementing the guidance law online in practice.

To better illustrate, involute trajectories with different impact angles (-135° , -45° , 45° , 135° deg) are presented in Fig. 5. It can be seen that by using involute trajectories, missiles can reach the target from any direction. It can also be seen that the launch angle decreases as the impact angle increases from negative to positive values. More analyses will be presented in the final subsection of this section.

Then, by substituting the value of γ_L back into (13), a can be easily obtained as

$$a = \frac{x_L - x_T}{\cos \gamma_T - \cos \gamma_L - (\gamma_L - \gamma_T) \sin \gamma_L} = \frac{y_L - y_T}{\sin \gamma_T - \sin \gamma_L + (\gamma_L - \gamma_T) \cos \gamma_L}. \quad (15)$$

Since $x_L = x_T$ and $y_L = y_T$ will not occur at the same time before the collision, there must exist a value of a that is not equal to zero. It should be noted that if $a \leq 0$, the involute trajectory does not exist. When $a > 0$, substituting the value of a in (11) yields the position of the center of the circle, which is used to perform the geometrical rule mentioned in the previous section. The arc length of an involute is given by $S_1(\varphi) = (1/2)a\varphi^2$ [34], which can be used to calculate the impact time after finding the desired trajectory.

As discussed above, if the target is assumed to be at the involute's end, it is also on the base circle. As a result, it can be seen from (11) that the position of O' is determined only by a given a desired impact angle. Although different values of a correspond to different involutes on the plane, this prescribes only one degree of freedom to design the trajectory. There are also some other curves that have one degree of freedom and can be used for impact angle control, such as a circle [9] or an Archimedean spiral [13]. Fig. 6 compares the trajectories using these two curves as opposed to the proposed circle involute for impact angle control. The impact angles corresponding to the upper three and

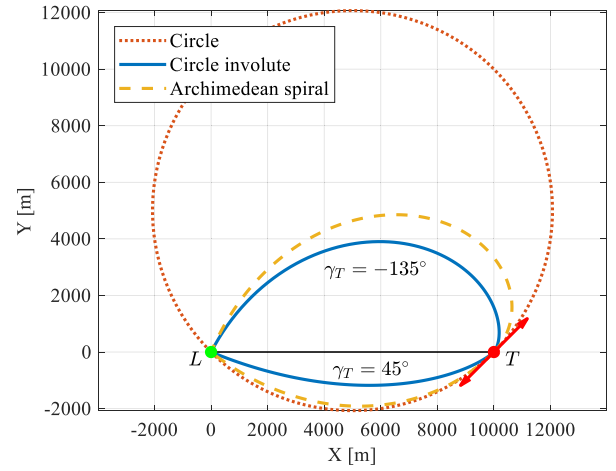


Fig. 6. Trajectories of different kinds of curves for the same impact angles.

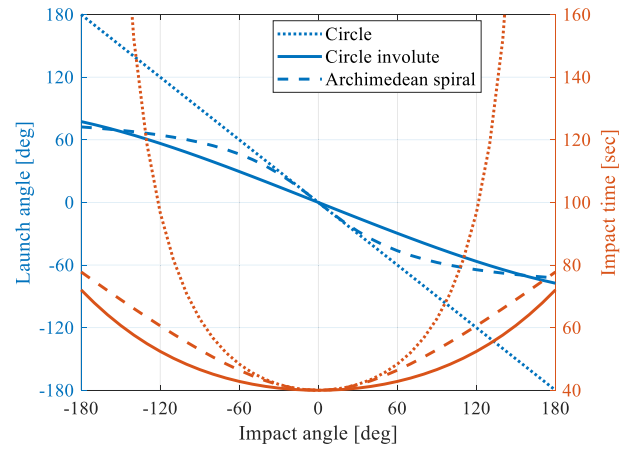


Fig. 7. Variations of launch angle and impact time of the three curves with respect to impact angle (orange lines: impact time; blue lines: launch angle).

lower three trajectories are -135° and 45° , respectively. It can be seen that the length of the circle trajectory is longer than the other two, especially for large impact angles, and this is consistent with the comparison between the circle and involute trajectories shown in [12]. Among these three kinds of curves, the trajectory of an involute of a circle has the shortest length, which leads to a shorter impact time.

The variations of the launch angle and impact time of the three kinds of curves with respect to impact angles are presented in Fig. 7. The missile is assumed to travel from (0, 0) to (10, 0) km at a constant speed $V_M = 250$ m/s. It is shown that for the same impact angle, the circle trajectory has the longest route (longer impact time than others) and the largest launch angle. In contrast, the involute trajectory results in the shortest flight time due to its shortest trajectory length. Except for impact angles near $\pm 180^\circ$, the involute trajectory also has the smallest launch angle for the same impact angle. Another feature is that the impact time increases gradually with the increased impact angle by using involute and spiral trajectories, while it raises dramatically by using circular trajectories. Note that such one degree of

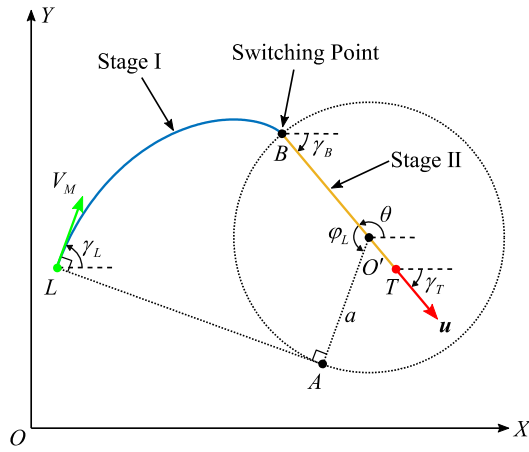


Fig. 8. Geometry of the two-stage trajectory.

freedom approaches sometimes limit the implementation of the constrained guidance mission, an improved two-stage approach is proposed to remove this restriction in the next subsection.

B. Two-Stage Approach for Launch and Impact Angle Constraints

In this subsection, an improved approach that yields explicit solutions for the two-stage trajectory satisfying both the launch angle and impact angle constraints is proposed. Note that in the previous general approach, the desired impact angle is achieved at the involute's end. This means that if the missile's lateral force was removed from this moment on, it would keep traveling in this direction, and hit any target in this direction with the desired impact angle. Motivated by this simple property, the general approach is improved by adding an extended straight line to the involute trajectory.

As shown in Fig. 8, the involute's end, denoted as B , becomes the switching point of the two-stage trajectory, and points B , O' , and T are colinear. In the first stage (depicted as Stage I), the missile travels from the launcher along the involute toward B . The missile's flight-path angle at B , denoted as γ_B , is the same as the desired impact angle on the target, which means that $\gamma_B = \gamma_T$. In the second stage (depicted as Stage II), the missile keeps its flight direction unchanged and hits the target with the desired impact angle.

Note that in the second stage, the missile travels from B along a straight line toward T , so that B is defined as

$$\mathbf{B} = \mathbf{T} - b\mathbf{u} = (x_T - b \cos \gamma_T, y_T - b \sin \gamma_T) \quad (16)$$

where $b \geq 0$ is a parameter that needs to be determined, namely, the second degree of freedom. When $b = 0$, (16) becomes $\mathbf{T} = \mathbf{B}$, which means the target is at the involute's end, and this kind of engagement has been discussed in the previous subsection. As a result, the two-stage trajectory only makes sense when $b > 0$.

Since B is located on the circle, O' is expressed as

$$\begin{aligned} \mathbf{O}' &= \mathbf{B} + a\mathbf{u} = \mathbf{T} + (a - b)\mathbf{u} \\ &= (x_T + (a - b) \cos \gamma_T, y_T + (a - b) \sin \gamma_T). \end{aligned} \quad (17)$$

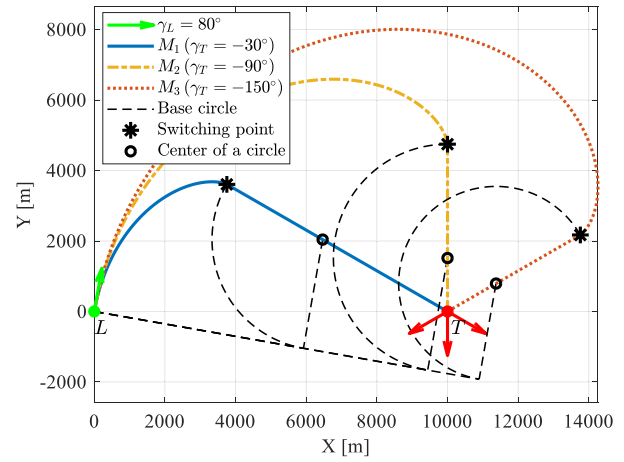


Fig. 9. Illustration of two-stage trajectories with different impact angles and the same launch angle.

The advantage of this two-stage approach is that the position of the circle center (O') is no longer only determined by the radius of the circle (a), and this is owing to the newly introduced second degree of freedom b .

By substituting (17) in (6), the parametric equations for the involute become

$$\begin{cases} x = x_T + (a - b) \cos \gamma_T - a(\cos(\varphi + \gamma_T) + \varphi \sin(\varphi + \gamma_T)) \\ y = y_T + (a - b) \sin \gamma_T - a(\sin(\varphi + \gamma_T) - \varphi \cos(\varphi + \gamma_T)) \end{cases} \quad (18)$$

Note that when $\varphi = \varphi_L$, launcher $L(x_L, y_L)$ is on the involute. Substituting $\varphi_L = \gamma_L - \gamma_T$ and $(x, y) = (x_L, y_L)$ into (18) yields

$$\begin{cases} x_L = x_T + (a - b) \cos \gamma_T - a \cos \gamma_L - a(\gamma_L - \gamma_T) \sin \gamma_L \\ y_L = y_T + (a - b) \sin \gamma_T - a \sin \gamma_L + a(\gamma_L - \gamma_T) \cos \gamma_L \end{cases} \quad (19)$$

By solving (19), a and b are obtained, respectively, as

$$a = \frac{(x_T - x_L) \sin \gamma_T - (y_T - y_L) \cos \gamma_T}{(\gamma_L - \gamma_T) \cos(\gamma_L - \gamma_T) - \sin(\gamma_L - \gamma_T)} \quad (20)$$

$$b = \frac{(x_T - x_L) \sin \gamma_L - (y_T - y_L) \cos \gamma_L - a(\gamma_L - \gamma_T \sin(\gamma_L - \gamma_T))}{\sin(\gamma_L - \gamma_T)}. \quad (21)$$

It should be noted that if $a \leq 0$ or $b \leq 0$, the two-stage trajectory does not exist. If not, substituting the values of a and b in (17) yields the position of the circle center, which is used to perform the geometrical rule defined by (9). It should also be noted that the general approach described in the previous subsection becomes a particular case of the two-stage approach by setting $b = 0$. As a result, the involute trajectories generated by the general approach are a subset of the two-stage trajectories, and apparently, the latter one has a wider range of applications.

To better illustrate the two-stage guidance approach for the launch and impact angle constraints, three engagement scenarios with different impact angles and the same launch angle are shown in Fig. 9. As shown in Fig. 9, in the first stage, the involute trajectory is responsible for imposing the desired impact angle. The missile's flight-path angle is

already equal to the desired impact angle at the switching point. In the second stage, the missile flies directly to the target at the desired impact angle. It can be seen that the proposed two-stage approach has the ability to achieve relatively larger impact angles as well. In addition, different impact angles can be achieved by the same launch angle.

C. Two-Stage Approach for Impact Time and Impact Angle Constraints

In this subsection, the approach to find a two-stage trajectory that satisfies both impact time and angle constraints is described. The trajectory geometry is shown in Fig. 8. For a two-stage trajectory, the lengths of the involute segment and straight segment are denoted as S_1 and S_2 , respectively. In the first stage, the arc length of an involute defined by (4) is $S_1(\varphi) = (1/2)a\varphi^2$ [34]. Since the involute starts from $\varphi = \varphi_L$ and ends at $\varphi = 0$, S_1 can be obtained as $S_1 = (1/2)a(\gamma_L - \gamma_T)^2$. In the second stage, the length of the straight trajectory is equal to the distance between the switching point and target. According to the definition in (16), S_2 is given by $S_2 = b$.

Then, the length of the two-stage trajectory, denoted as S , can be written as

$$S = S_1 + S_2 = \frac{1}{2}a(\gamma_L - \gamma_T)^2 + b. \quad (22)$$

For the constant speed considered in this work (a general assumption in homing guidance literature), the length of the trajectory is directly correlated with the impact time. Once the trajectory is determined, the impact time t_f can be obtained by using (22) as

$$t_f = \frac{S}{V_M} = \frac{a(\gamma_L - \gamma_T)^2 + 2b}{2V_M}. \quad (23)$$

Substituting (20) and (21) into (23) yields

$$\begin{aligned} & \frac{(x_T - x_L) \sin \gamma_T - (y_T - y_L) \cos \gamma_T}{(\gamma_L - \gamma_T) \cos(\gamma_L - \gamma_T) - \sin(\gamma_L - \gamma_T)} \\ & \times \left[\frac{(\gamma_L - \gamma_T)^2}{2} - \frac{\gamma_L - \gamma_T - \sin(\gamma_L - \gamma_T)}{\sin(\gamma_L - \gamma_T)} \right] \\ & + \frac{(x_T - x_L) \sin \gamma_L - (y_T - y_L) \cos \gamma_L}{\sin(\gamma_L - \gamma_T)} - V_M t_f = 0. \end{aligned} \quad (24)$$

As seen in (24), the impact time t_f is only related to γ_L given the launcher and target locations. Therefore, different impact times can be achieved by finding proper launch angles. Given a pair of $t_f = t_{des}$ and γ_T , the corresponding γ_L can be obtained by solving (24) numerically (like Newton's method). Similar to the calculation of (14), this process can be done offline before launch and therefore will not cause computation issues in implementing the guidance law online. Then, the parameters a and b are obtained explicitly by substituting the value of γ_L back into (20) and (21), respectively. If $a > 0$ and $b > 0$, the position of the circle center, which is used to perform the geometrical rule defined by (9), can be obtained by (17).

For a better understanding of the two-stage guidance with impact time and angle constraints, three engagement

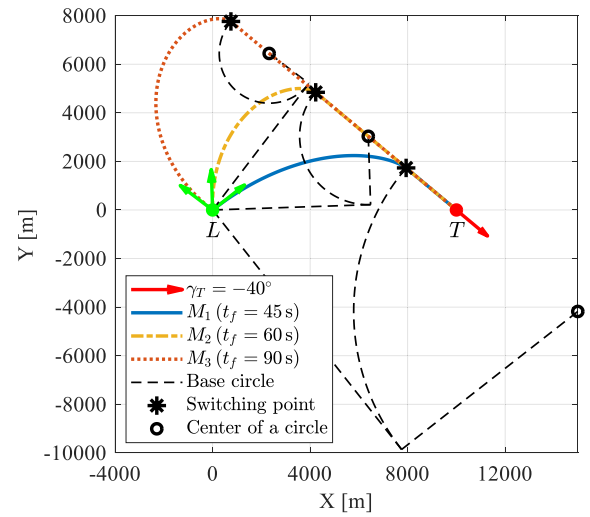


Fig. 10. Illustration of two-stage trajectories with different impact times and the same impact angle.

scenarios with different impact times and the same impact angle are shown in Fig. 10. As seen in Fig. 10, in the first stage, the missile travels along the involute trajectory toward the switching point. At the switching point, the missile's flight-path angle is equal to the desired impact angle, and then, the missile flies directly to the target in the second stage. It can also be seen that the distance between the switching point and the target increases as the impact time increases in this case. Meanwhile, a longer impact time corresponds to a larger launch angle to generate a feasible involute trajectory. Due to the same desired impact angle, the switching points in the three scenarios are co-linear.

D. Analysis of Achievable Constraints

In this subsection, the ranges of different constraints that can be achieved are presented. The one-stage involute trajectories with one constraint are analyzed first. Then, the analyses of two-stage trajectories with two constraints are presented.

One-stage trajectory: As for a one-stage involute trajectory, the launch angle and impact time are uniquely determined by a desired impact angle. First, the influence of different initial engagement scenarios is analyzed. The relative position of the missile with respect to the target is described by r and λ . By using the initial LOS angle λ_L , (14) can be rewritten as

$$\begin{aligned} & (\sin \gamma_T - \sin \gamma_L + (\gamma_L - \gamma_T) \cos \gamma_L) \\ & - \tan \lambda_L (\cos \gamma_T - \cos \gamma_L - (\gamma_L - \gamma_T) \sin \gamma_L) = 0. \end{aligned} \quad (25)$$

It can be seen that for a pair of impact angle and initial LOS angle, the launch angle can be uniquely determined. In other words, engagement scenarios with the same initial LOS angle share the same one-to-one correspondence between the launch angle and impact angle, regardless of the initial relative range.

For better illustration, Fig. 11 shows the variations of the launch angle and impact time of the involute trajectories

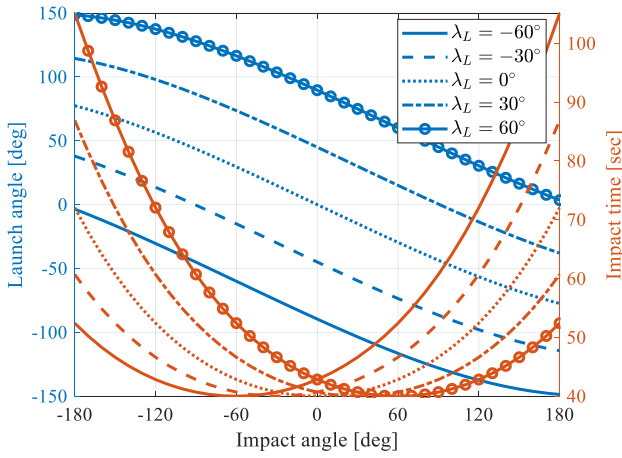


Fig. 11. Variations of the launch angle and impact time of the involute trajectories with respect to impact angles for different initial LOS angles (orange lines: impact time; blue lines: launch angle).

with respect to impact angles for different initial LOS angles (-60° , -30° , 0° , 30° , 60°) at the same initial relative range (10 000 m). The missile is assumed to travel at a constant speed $V_M = 250$ m/s. In this case, it can be seen that for the same impact angle, the launch angle increases as the initial LOS angle increases from -60 to 60 degrees. As for impact time, the minimum impact time occurs when the desired impact angle equals the initial LOS angle, under which circumstance the missile will fly directly to the target.

Two-stage trajectory: For this case, the correspondence between the launch angle and impact angle as well as the correspondence between the impact time and impact angle under the current engagement scenario are analyzed.

As seen in Fig. 10, for a specified impact angle, both the launch angle and trajectory length increase as the switching point moves away from the target. Starting from the target position, as the switching point moves in the opposite direction of the desired impact direction, the LOS angle between the missile and switching point, denoted as λ_S , changes from $\lambda_S = \lambda_L$ to $\lambda_S = \gamma_T + \pi$, $\gamma_T \in [-\pi, 0]$ or $\lambda_S = \gamma_T - \pi$, $\gamma_T \in (0, \pi)$. Recall the analysis of one-stage trajectories, for a specified impact angle, the launch angle increases as the initial LOS angle increases and is independent of the relative range. Therefore, the minimum launch angle is achieved when the switching point coincides with the target, which leads to an involute trajectory without the second stage. The maximum launch angle is achieved when the switching point is infinitely far away from the target. The upper and lower bounds of the launch angle for a specified impact angle can be calculated by (25), and the results of scenarios with $\lambda_L = 0$ are shown in solid and dashed lines in Fig. 12.

Next, the trend of the impact time is analyzed. For a given engagement scenario, the trajectory is uniquely determined by a pair of launch and impact angles. For a specified impact angle, as seen in Fig. 10 and (22), the trajectory length increases as the launch angle increases, and this leads to a longer impact time for a constant speed

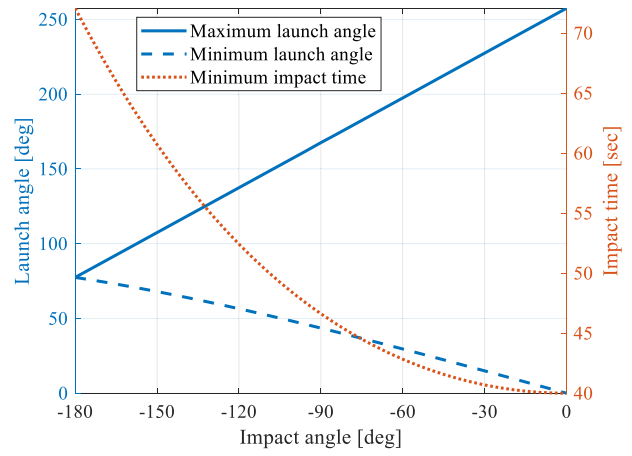


Fig. 12. Possible launch angles and impact times with respect to impact angles (two-stage trajectory, $\lambda_L = 0$; orange line: impact time; blue lines: launch angle).

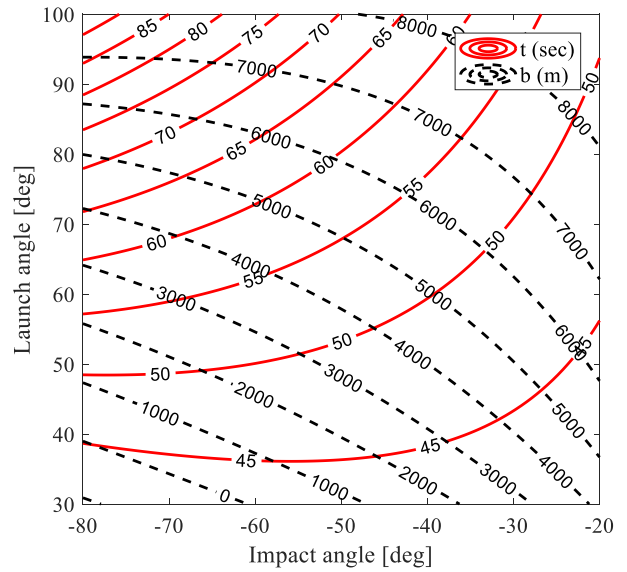


Fig. 13. Contours of impact time and parameter b for various launch angles and impact angles (two-stage trajectory).

vehicle. Therefore, the minimum impact time for a specified impact angle is achieved at the minimum launch angle, which leads to an involute trajectory without the second stage. The minimum impact time for a vehicle that travels from $(0, 0)$ to $(10, 0)$ km at a constant speed $V_M = 250$ m/s is presented in a dotted line in Fig. 12. By moving the switching point away from the target, any impact time longer than the minimum impact time is achievable.

To better illustrate, the contours of impact time and parameter b (representing the length of the second stage) for various launch angles and impact angles are presented in Fig. 13. For a better visibility, the ranges of impact angles and launch angles are chosen to be $[-80, -20]$ and $[30, 100]$ deg, respectively. As expected, for the same impact angle, the impact time and parameter b increase as the launch angle increases. It should be noted that the minimum impact time is achieved when $b = 0$, and the combinations

of the launch and impact angles below the contour $b = 0$ are not feasible. Another observation is that the impact time contours become denser for large launch angles and impact angles.

V. GUIDANCE LAW DESIGN

In this section, the guidance law is designed such that the missile travels along the desired trajectory. First, a two-stage involute-based guidance (TIG) law is presented to maintain the missile along the desired two-stage trajectory. Then, a robust two-stage involute-based guidance (RTIG) law is proposed considering the external disturbances and initial heading errors. Both TIG and RTIG laws consist of two stages. In the first stage, the guidance law aims to maintain the missile along the involute trajectory and reach the switching point with a desired velocity direction. Once the switching condition is satisfied, guidance law in the second stage is employed to ensure the capture of the target.

A. Two-Stage Involute-Based Guidance Law

In this subsection, the TIG law is presented to maintain the missile along the desired trajectory. In the first stage, in order to travel along the involute, the missile's lateral acceleration is required to be

$$A_M(\varphi) = -V_M^2 \kappa(\varphi) = -\frac{V_M^2}{a\varphi} \quad (26)$$

where $\kappa(\varphi) = 1/(a\varphi)$ is the curvature of the involute [34]. Substituting $\varphi = \gamma - \gamma_T$ (8) into (26) yields

$$A_M = -\frac{V_M^2}{a(\gamma - \gamma_T)}. \quad (27)$$

Therefore, after getting the parameter a through (20), the TIG law for the involute trajectory can be obtained. In the second stage, the PNG law is employed to hit the target

$$A_M = NV_M \dot{\lambda} \quad (28)$$

where N denotes the effective navigation gain, which is usually set in the range of 3–5. The switching logic between the above two guidance laws is proposed as follows:

$$A_M = \begin{cases} -\frac{V_M^2}{a(\gamma - \gamma_T)}, & \text{if } |\varphi| > \zeta \\ NV_M \dot{\lambda}, & \text{if } |\varphi| \leq \zeta \end{cases} \quad (29)$$

where φ is defined by (8), namely, the deviation between the missile's flight-path angle and the desired impact angle. ζ denotes the minimal tolerance for the impact angle error. Note that the involute guidance law in the first stage has guaranteed $\varphi \rightarrow 0$, which means that there must exist an acceptable tolerance ζ that can be met.

B. Robust Two-stage Involute-based Guidance Law

The successful implementation of the TIG law depends on the assumption that the missile is on the involute and $\gamma = \gamma_L$ at the initial moment. If the assumption is violated, the TIG law cannot guide the missile back to the desired

trajectory. Meanwhile, it should be noted that the TIG law cannot compensate the external disturbances. Therefore, an RTIG law considering external disturbances and initial heading errors should be designed. Specifically, an SMC-based RTIG law is presented in this subsection considering the external disturbances and initial heading errors.

Stage I: When there are external disturbances and initial heading errors, the missile will deviate from the desired trajectory, and the geometrical rule given by (9) will no longer be satisfied. To ensure the missile tracks the desired trajectory, the well-known sliding-mode controller is employed to enforce the geometrical rule during the first stage. Consider uncertain external disturbances (such as wind disturbances and process noise, denoted as w) [13] affecting the system as follows:

$$\dot{\gamma} = \frac{A_M + w}{V_M}. \quad (30)$$

Based on the geometrical rule defined by (9), the sliding surface is designed as

$$s_1 = \tan \delta - \gamma + \gamma_T. \quad (31)$$

Taking the time derivative of (31) and using $\delta = \gamma - \lambda_{O'}$ lead to

$$\dot{s}_1 = \frac{\sec^2 \delta - 1}{V_M} A_M + \frac{\sec^2 \delta - 1}{V_M} w - \dot{\lambda}_{O'} \sec^2 \delta. \quad (32)$$

Let the sliding-mode controller be composed of two parts, an equivalent controller A_M^{eq} and a discontinuous controller A_M^{disc} , so that

$$A_M = A_M^{eq} + A_M^{disc}. \quad (33)$$

The equivalent controller is designed as $A_M^{eq} = V_M \dot{\lambda}_{O'} \sec^2 \delta / (\sec^2 \delta - 1)$. The discontinuous controller is designed as $A_M^{disc} = -k_1 \text{sign}(s_1)$, where $k_1 > 0$ is a parameter to be designed. Then, the guidance law for the involute trajectory in the first stage can be obtained as

$$A_M = \frac{V_M}{\sec^2 \delta - 1} \dot{\lambda}_{O'} \sec^2 \delta - k_1 \text{sign}(s_1). \quad (34)$$

To implement the above guidance law in practice, δ is obtained by using (10) as $\delta = \gamma - \lambda_{O'}$, and $\dot{\lambda}_{O'}$ is obtained by substituting (17) into (10) as

$$\dot{\lambda}_{O'} = \tan^{-1} \frac{y_T - y + (a - b) \sin \gamma_T}{x_T - x + (a - b) \cos \gamma_T} \quad (35)$$

and then taking the time derivative of (35), which is shown in (36) given at the bottom of the next page.

As discussed in the previous section, parameters a and b can be obtained before implementing the guidance law. With the stationary target's location (x_T, y_T) and constant missile speed V_M provided in advance, the real-time guidance information required to implement the guidance law are the missile's current location (x, y) and flight-path angle γ .

To prove the stability of the system, a candidate Lyapunov function is selected as $W = (1/2)s_1^2$. Taking the time

derivative of W yields

$$\begin{aligned}\dot{W} &= s_1 \dot{s}_1 = s_1 (-k_1 \text{sign}(s_1) + w) \frac{\sec^2 \delta - 1}{V_M} \\ &\leq -|s_1| (k_1 - |w|) \frac{\sec^2 \delta - 1}{V_M}.\end{aligned}\quad (37)$$

It can be seen from (37) that as long as $k_1 > \max(|w|)$, the sliding surface variable reaches the origin in finite time. Once the sliding surface is reached, the geometrical rule can be enforced.

Stage II: In the second stage, similar to the first stage, a sliding-mode controller is proposed to ensure the capture of the target under external disturbances. The sliding surface is designed as $s_2 = \dot{\lambda}$, and taking the time derivative of s_2 leads to

$$\dot{s}_2 = \frac{\dot{r}}{r V_M} A_M + \frac{\dot{r}}{r V_M} w - \frac{2\dot{r}\dot{\lambda}}{r}. \quad (38)$$

Similar to the derivation in the first stage, the guidance law in the second stage is designed as

$$A_M = 2V_M \dot{\lambda} + k_2 \text{sign}(s_2) \quad (39)$$

where $k_2 > 0$ is a parameter to be designed. Following the similar proof in Stage I, the sliding surface variable can reach the origin in finite time when $k_2 > \max(|w|)$.

Switching logic: The switching logic between the above two guidance laws is proposed as follows:

$$A_M = \begin{cases} \frac{V_M}{\sec^2 \delta - 1} \dot{\lambda}_O \sec^2 \delta - k_1 \text{sign}(s_1), & \text{if } |\varphi| > \zeta \\ 2V_M \dot{\lambda} + k_2 \text{sign}(s_2), & \text{if } |\varphi| \leq \zeta \end{cases} \quad (40)$$

where φ is defined by (8), namely, the deviation between the missile's flight-path angle and the desired impact angle. ζ denotes the minimal tolerance for the impact angle error. Note that the involute guidance law in the first stage has guaranteed $\varphi \rightarrow 0$, which means that the minimal tolerance ζ can always be met. In addition, the discontinuous function $\text{sign}(s)$ in (40) can be replaced by the function $\tanh(s)$ to reduce chattering while implementing the guidance law in practice.

Block diagram for the guidance law: For a better understanding of the aforementioned guidance law, the block diagram describing the complete design of the RTIG law is shown in Fig. 14. To begin with, the center of the base circle of the involute is obtained via simple calculations according to the initial conditions and final constraints. Then, the locations of the missile and the center of the circle are used in the geometrical rule defined by (9), which is later implemented by the guidance law in (34) in Stage I. As a result, the missile will travel along the involute trajectory toward the involute's end with the desired velocity direction. Once the switching logic in (40) is satisfied, the guidance law in (39) that nullifies the LOS rate is employed in Stage

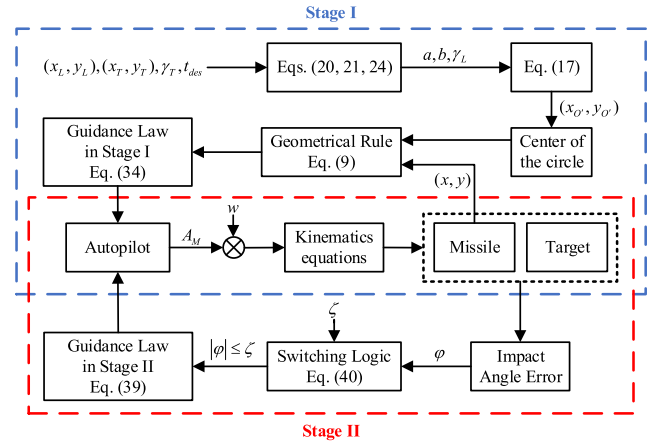


Fig. 14. Block diagram for the RTIG law.

II for intercepting the target with near-zero acceleration. In both stages, the external disturbances are introduced into the system by adding w to the guidance command A_M .

VI. SIMULATION RESULTS AND ANALYSIS

In this section, the performance of the proposed guidance strategy is investigated via a series of numerical simulations. First, the scenario with no external disturbance is simulated by using the proposed TIG law. Then, the proposed RTIG law is evaluated in the presence of disturbances and initial heading errors. Meanwhile, Monte Carlo simulations are carried out to verify the robustness of the RTIG law. The feasibility of constraints under different acceleration limits is also analyzed. Finally, the proposed RTIG law is compared with another similar two-stage guidance law in [33] and the geometric-based EG in [28].

In all cases, without additional explanation, the locations of the launcher and target in the inertial Cartesian frame are (0, 0) and (10, 0) km, respectively. The missile is assumed to travel at a constant speed $V_M = 250$ m/s, and the acceleration of the missile is bounded by $A_{M \max} = 50$ m/s². As for the switching logic, the minimal tolerance for the impact angle error ζ is selected as 0.01° . Finally, the allowable miss distance is set to be less than 1 m.

A. TIG Law for Various Impact Times and Impact Angles

In this subsection, the interception of the target via the TIG law given by (29) is simulated for different impact times and impact angles. The simulations are conducted in an ideal environment without disturbances. The effective navigation gain for the PNG law used in the second stage is set as $N = 3$. The desired impact angle and time, and trajectory parameters for four missiles are listed in Table I, where γ_T and t_{des} are specified while γ_L , a , and b are calculated. The results of the simulations are presented in Fig. 15.

$$\dot{\lambda}_O = V_M \frac{\cos \gamma (y_T - y + (a - b) \sin \gamma_T) - \sin \gamma (x_T - x + (a - b) \cos \gamma_T)}{(x_T - x + (a - b) \cos \gamma_T)^2 + (y_T - y + (a - b) \sin \gamma_T)^2}. \quad (36)$$

TABLE I
Desired Impact Angles/Times and Trajectory Parameters for TIG
Simulations

Guidance law	γ_T , deg	t_{des} , sec	γ_L , deg	a , m	b , m
TIG	-35	50	64.19	4539.4	5698.1
TIG	-35	65	113.14	2105.8	9211.6
TIG	-70	65	75.94	3519.2	4834.2
TIG	-70	80	94.97	3091.1	7187.9

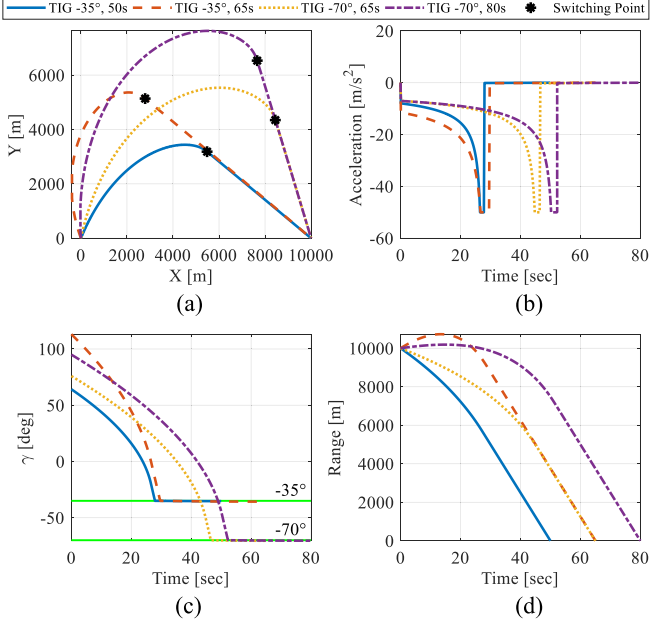


Fig. 15. Simulation results for various impact times and impact angles via TIG law. (a) Flight trajectories. (b) Missile acceleration trends. (c) Flight-path angle variations. (d) Relative range histories.

It can be seen from Fig. 15 that all the missiles succeed to intercept the target at the desired impact time and angle. The trajectories of four missiles are presented in Fig. 15(a), which shows that the switching points of the trajectories that share the same γ_T are colinear. For the same γ_T , a longer t_{des} results in larger values of b and γ_L . By inspecting Fig. 15(b), the missile's acceleration saturates at the switching point because the denominator in (27) tends to zero as $\gamma \rightarrow \gamma_T$. But the saturation only lasts for a very short time and then the guidance law switches to the PNG (28) to generate zero acceleration in the second stage, which naturally results in zero control effort. As shown in Fig. 15(c), the missile's flight-path angle can meet the desired value and keeps the same value in the second stage. From Fig. 15(d), it is clearly shown that the relative range can converge to zero at the desired impact time. The initial increase of the relative range for TIG (-35°, 65s) is caused by its relatively large launch angle. This is in accordance with the geometric property of the involute trajectory.

B. RTIG Law With Disturbances and Initial Heading Errors

In this subsection, the robustness of the RTIG law is evaluated under practical engagement conditions, followed

TABLE II
Desired Impact Angles/Times and Trajectory Parameters for RTIG
Simulations

Guidance law	γ_T , deg	t_{des} , sec	γ_L , deg	a , m	b , m
RTIG	-35	50	64.19	4539.4	5698.1
TIG	-35	50	64.19	4539.4	5698.1
RTIG	-70	65	75.94	3519.2	4834.2
TIG	-70	65	75.94	3519.2	4834.2

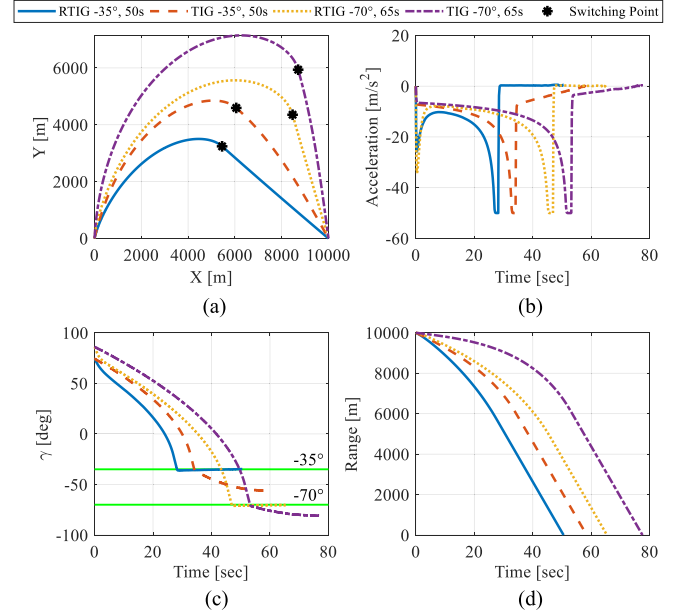


Fig. 16. Simulation results for RTIG and TIG laws with disturbances and initial heading errors. (a) Flight trajectories. (b) Missile acceleration trends. (c) Flight-path angle variations. (d) Relative range histories.

by a set of Monte Carlo simulations. First, the time lag due to the missile autopilot is considered assuming the first-order dynamics with the time constant 0.1 s. The external disturbance described by w is assumed to follow a uniform distribution of -10 to 10 m/s². Meanwhile, an initial heading error $\Delta\gamma_L = 10^\circ$ is considered. Based on the results shown in Section V-B, the gain of the sliding-mode controller is chosen as $k_1 = k_2 = 30$ to ensure the stability of the system. Two scenarios using the TIG law (-35°, 50 s and -70°, 65 s) in Table I are chosen as the comparison cases to show the effectiveness of the RTIG law under practical engagement conditions. The desired impact angle and time, and trajectory parameters for four missiles are listed in Table II, where γ_T and t_{des} are specified while γ_L , a , and b are calculated. The results of the simulations are presented in Fig. 16.

It is clearly shown in Fig. 16 that by using the RTIG law, missiles can hit the target at both desired impact angles and desired impact times in the presence of disturbances and initial heading errors. In contrast, missiles using the TIG law fail to satisfy the constraints. The trajectories of four missiles are presented in Fig. 16(a). The trends of each missile's acceleration are given in Fig. 16(b). For missiles

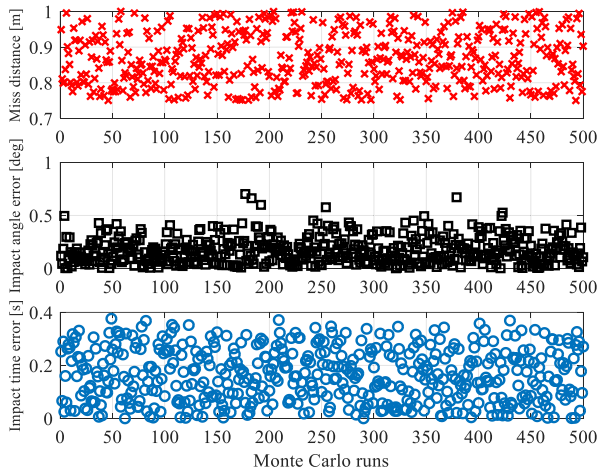


Fig. 17. Monte Carlo results for the missile using the RTIG law with the constraints $(-70^\circ, 65 \text{ s})$.

using the RTIG law, the missile's acceleration has a dip at the beginning due to the initial heading error but returns to normal quickly. It can be seen from Fig. 16(c) that only by using the RTIG law, the missile's flight-path angle can achieve the desired value. As shown in Fig. 16(d), the relative range in each scenario converges to zero, however, only missiles using the RTIG law succeed to intercept the target at the desired impact time.

Monte Carlo Simulations of the RTIG Law: To better verify the robustness of the RTIG law, 500 Monte Carlo simulations are carried out under external disturbances and initial heading errors. The engagement conditions are chosen to be the same as those for the missile RTIG $(-70^\circ, 65 \text{ s})$ listed in Table II in Section VI-B. The external disturbance described by w is assumed to follow a uniform distribution in $[-10, 10] \text{ m/s}^2$. The initial heading error is assumed to follow a uniform distribution in $[-10, 10] \text{ deg}$. Meanwhile, the gain of the sliding-mode controller is chosen as $k_1 = k_2 = 30$. The distributions of the miss distance, impact time error, and impact angle error in each simulation are presented in Fig. 17. It can be seen that all the miss distances are within 1 m, which meets the allowable miss distance setting. In addition, the impact angle errors are around 0.15 deg, and the impact time errors are around 0.16 s, which show the strong robustness of the RTIG law against external disturbances and initial heading errors. Additional Monte Carlo simulations are also performed for other cases (omitted here for brevity), and the results also demonstrate the robustness of the RTIG law.

C. Feasibility Analysis Under Acceleration Limit

In this subsection, the capture regions under different acceleration limits are analyzed. For a given engagement scenario, the theoretical capture region can be obtained by the procedure presented in Section IV-D. In practical implementation, the acceleration limit will affect the theoretical capture region. Fig. 18 shows the simulation results of capture regions with different acceleration limits under the current engagement scenario ($L = (0, 0) \text{ km}$,

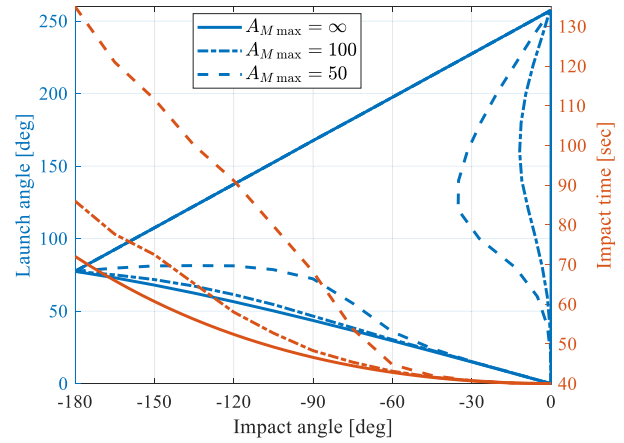


Fig. 18. Capture regions under different acceleration limits (orange lines: impact time; blue lines: launch angle).

$T = (10, 0) \text{ km}$, $V_M = 250 \text{ m/s}$). A mission is considered successful if the impact angle error is less than 1 degree.

The lower boundary of the capture region of launch angles given by a solid blue line (theoretical, $A_{M \max} = \infty \text{ m/s}^2$) represents the involute trajectories without the second stage. In this case, because of the large required acceleration near the collision, the constraint may not be satisfied under a small acceleration limit, especially for large desired impact angles. For a specified impact angle, a larger launch angle leads to a two-stage trajectory with a longer second segment. It should be noted that the acceleration saturation takes place at the switching point, rather than near the collision, which ensures successful interception that is guaranteed by the second-stage guidance law and not affected by saturation. Recall that the minimum impact time is achieved at the minimum launch angle. If the minimum launch angle increases due to saturation in practical implementation, the corresponding minimum impact time is longer than the theoretical one shown as the solid orange line.

The unachievable area on the right of the capture region corresponds to scenarios with small impact angles and large launch angles. For a surface-to-surface scenario ($L = (0, 0) \text{ km}$, $T = (10, 0) \text{ km}$), it is difficult for the missile to turn around. Meanwhile, the contours of parameter a (radius of the base circle) for this area are presented in Fig. 19. As seen in (26), a smaller value of parameter a leads to larger nominal acceleration. The boundary of the capture region is in line with the distribution of parameter a . Finally, it should be noted from Fig. 18 that if the acceleration limit is $A_{M \max} = 100 \text{ m/s}^2$, the capture region is very close to the theoretical one.

D. Comparison Study

Comparison Study I: First, the proposed guidance law is compared with the ITAG law in [33], which consists of an IAG law in the first stage and a PNG law with a straight line in the second stage. The simulation condition is chosen to be the same as the one in [33]: the initial locations of the launcher and target are $(0, 0.5)$ and $(11, 0) \text{ km}$, respectively;

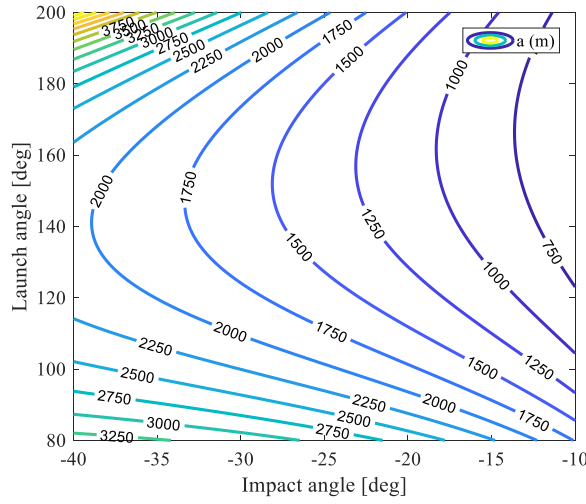


Fig. 19. Contours of parameter a for various launch angles and impact angles (two-stage trajectory).

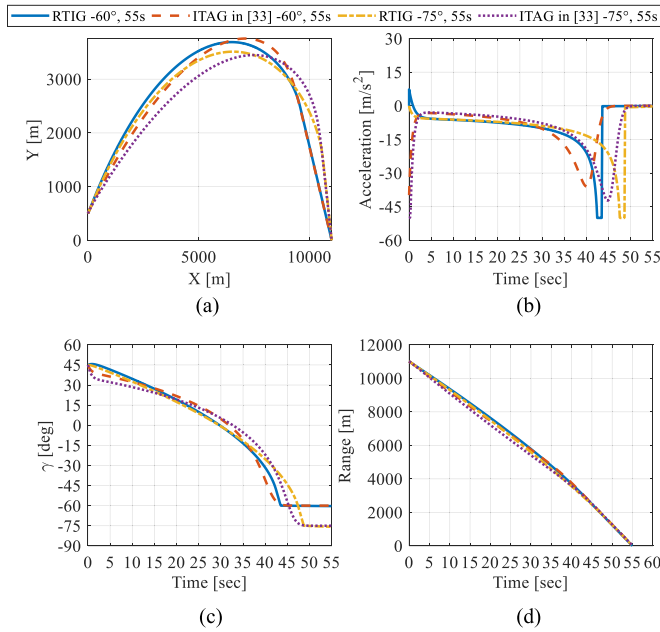


Fig. 20. Comparison study of the RTIG law and ITAG law [33]. (a) Flight trajectories. (b) Missile acceleration trends. (c) Flight-path angle variations. (d) Relative range histories.

the missile is assumed to travel at a constant speed $V_M = 250$ m/s; the initial launch angle is 45 deg; other simulation conditions are chosen to be the same as the previous settings.

The simulation results are presented in Fig. 20 for a selected impact time (55 s) and impact angles (-60° , and -75°). The trajectories of four missiles are shown in Fig. 20(a). By inspecting Fig. 20(b), each missile's acceleration turns to near-zero after the switching point. The acceleration of missiles using RTIG law saturates at the switching point but only lasts for a very short time. Note that the RTIG law requires much smaller initial acceleration than the ITAG law in [33]. As shown in Fig. 20(c), all the impact angles by both guidance laws can converge to their desired values in advance at the switching point and keep

TABLE III
Desired Impact Angles/Times and Launch Angles for
Comparison Study II

Guidance law	γ_T , deg	t_{des} , sec	γ_L^* , deg	γ_L , deg
RTIG	-60	100	134.5	124.9
EG			115.3	
RTIG	-120	100	95	86
EG			77	

them until the final interception. Note that in this work, the switching point can be obtained explicitly, while in [33] it requires numerical optimization. Finally, it can be seen from Fig. 20(d) that the relative range converges to zero at the desired impact time in each case.

Comparison Study II: The proposed RTIG law is also compared with the EG law given in [28]. Note that the EG law can impose three constraints (launch angle, impact angle, and impact time). However, to reduce computational complexity, an alternative approach is provided in [28] to find elliptical trajectories that satisfy impact angle and launch angle constraints or impact angle and impact time constraints, not all three constraints altogether. Thus, the proposed RTIG law is compared with the EG law that considers only the impact angle and impact time constraints. The simulation condition is chosen to be the same as the one in [28]: the locations of the launcher and target in the inertial Cartesian frame are (0, 0) and (10, 1) km, respectively; the missile is assumed to travel at a constant speed $V_M = 300$ m/s. The desired impact angles and times, and launch angles of two groups for comparison are listed in Table III. Note that γ_L^* denotes the corresponding launch angle calculated by the two guidance methods for a pair of desired impact time and angle. To impose the same level of heading error in each comparison group, the real launch angle γ_L is selected to be the average of the calculated launch angles of the two guidance methods. Other simulation conditions are chosen to be the same as the previous settings. The gains of the PID controller for the EG law are given in [28].

It can be seen from Fig. 21 that both RTIG and EG laws succeed to intercept the target at the desired impact time and angle. As shown in Fig. 21(a), the trajectory of the EG law is part of the ellipse while the trajectory of the RTIG law is a combination of the circle involute and straight line. The trends of each missile's acceleration are given in Fig. 21(b). It can be seen that during the initial phase, larger acceleration is created in each case due to the initial heading error. However, the initial acceleration of the EG law is saturated while the RTIG law is not. During the middle phase, except for the case EG (-120° , 100 s), the accelerations in other three cases are saturated. The reason is that when the curvature κ of the geometric curve is larger than a certain value, to be specific when $\kappa > A_{M\max}/V_M^2$, the acceleration required to track the curve exceeds the acceleration limit. For the EG law and RTIG law, the maximum curvature appears at the vertex of the ellipse and the involute's end, respectively. Fig. 21(c) presents

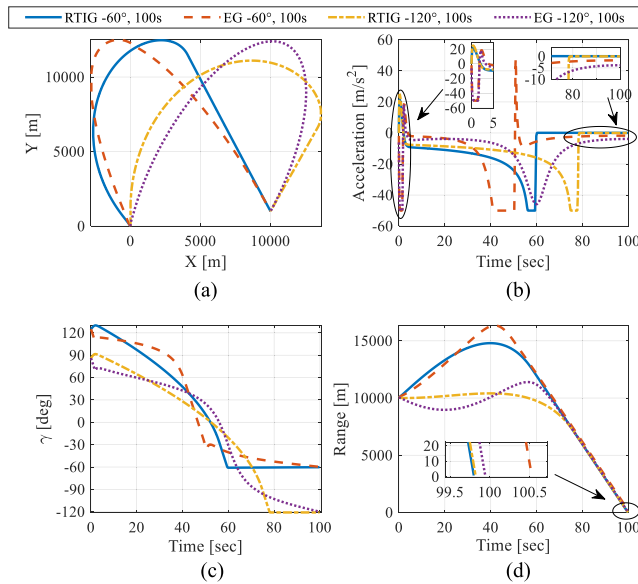


Fig. 21. Comparison study of the RTIG law and EG law. (a) Flight trajectories. (b) Missile acceleration trends. (c) Flight-path angle variations. (d) Relative range histories.

the flight-path angle variations of each missile. The initial slump or spike of γ is caused by each missile's maneuver to offset the initial heading error. In addition to satisfying an impact angle constraint at the final interception point like the EG law, the RTIG law can achieve the desired impact angle in advance, and keep it till the final interception point due to the two-stage strategy. Finally, it can be seen from Fig. 21(d) that the relative range can converge to zero for all four missiles, and the impact time errors are within the acceptable range.

VII. CONCLUSION

A two-stage switching guidance law is proposed for achieving the desired impact time and impact angle against a stationary target. By following a circle involute, the missile can reach the desired velocity direction at the end of the first stage. Then, it is switched to the guidance law that ensures zero LOS rate in the second stage. Explicit solutions for the trajectory's parameters are presented to generate the desired two-stage trajectory that meets both impact time and angle constraints. Compared with other ITAG laws, the proposed guidance law does not involve model linearization, time-to-go estimation, and numerical optimization routine. Another feature is that the proposed guidance law can achieve the desired impact angle before the interception point, such that zero acceleration is created and maintained in the second stage. Meanwhile, the achievable range of different constraints is analyzed considering practical issues such as initial launch angles, initial LOS angles, and acceleration limits. To implement the two-stage guidance law in practice, a sliding-mode-control-based robust two-stage guidance law is constructed with guaranteed

robustness. Numerical simulations under various engagement scenarios validate that the proposed guidance law is capable of meeting different impact angles with the same impact time and vice versa. In addition, simulations under practical conditions demonstrate that the proposed guidance law can not only achieve the desired constraints but also be robust to external disturbances, initial heading errors, and autopilot lag.

REFERENCES

- [1] M. Kim and K. V. Grider
Terminal guidance for impact attitude angle constrained flight trajectories
IEEE Trans. Aerosp. Electron. Syst., vol. AES-9, no. 6, pp. 852–859, Nov. 1973.
- [2] R. Chang-Kyung, C. Hangju, and T. Min-Jea
Time-to-go weighted optimal guidance with impact angle constraints
IEEE Trans. Control Syst. Technol., vol. 14, no. 3, pp. 483–492, May 2006.
- [3] P. Lu, D. B. Doman, and J. D. Schierman
Adaptive terminal guidance for hypervelocity impact in specified direction
J. Guid., Control, Dyn., vol. 29, no. 2, pp. 269–278, 2006.
- [4] R. Tekin and K. S. Erer
Switched-gain guidance for impact angle control under physical constraints
J. Guid., Control, Dyn., vol. 38, no. 2, pp. 205–216, 2015.
- [5] S. He and C. Lee
Optimal impact angle guidance for exoatmospheric interception utilizing gravitational effect
IEEE Trans. Aerosp. Electron. Syst., vol. 55, no. 3, pp. 1382–1392, Jun. 2019.
- [6] S. He, D. Lin, and J. Wang
Integral global sliding mode guidance for impact angle control
IEEE Trans. Aerosp. Electron. Syst., vol. 55, no. 4, pp. 1843–1849, Aug. 2019.
- [7] A. Dhabale and D. Ghose
Curvature constrained cubic spline impact angle guidance for intercepting stationary targets
IEEE Trans. Aerosp. Electron. Syst., vol. 54, no. 4, pp. 1750–1766, Aug. 2018.
- [8] M.-G. Yoon
Relative circular navigation guidance for three-dimensional impact angle control problem
J. Aerosp. Eng., vol. 23, no. 4, pp. 300–308, 2010.
- [9] R. Tsalik and T. Shima
Inscribed angle guidance
J. Guid., Control, Dyn., vol. 38, no. 1, pp. 30–40, 2015.
- [10] I. R. Manchester and A. V. Savkin
Circular navigation guidance law for precision missile/target engagements
J. Guid., Control, Dyn., vol. 29, no. 2, pp. 314–320, 2006.
- [11] T. Zhang and H. She
Elliptical trajectory guidance law with terminal impact angle constraint
in *Proc. AIAA Atmosph. Flight Mechanics Conf.*, 2015, Paper AIAA 2015–1021.
- [12] J. Wang, S. Zhong, and Y. Jiang
Involute guidance laws with terminal impact angle constraints
in *Proc. IEEE Chin. Guid., Navigat. Control Conf.*, 2016, pp. 192–197.
- [13] T. Tripathy and T. Shima
Archimedean spiral-based intercept angle guidance
J. Guid., Control, Dyn., vol. 42, pp. 1–11, 2018.

- [14] J. In-Soo, L. Jin-Ik, and T. Min-Jea
Impact-time-control guidance law for anti-ship missiles
IEEE Trans. Control Syst. Technol., vol. 14, no. 2, pp. 260–266, Mar. 2006.
- [15] D. Cho, H. J. Kim, and M.-J. Tahk
Nonsingular sliding mode guidance for impact time control
J. Guid., Control, Dyn., vol. 39, no. 1, pp. 61–68, 2016.
- [16] M. Kim, B. Jung, B. Han, S. Lee, and Y. Kim
Lyapunov-based impact time control guidance laws against stationary targets
IEEE Trans. Aerosp. Electron. Syst., vol. 51, no. 2, pp. 1111–1122, Apr. 2015.
- [17] O. Ariff, R. Zbikowski, A. Tsourdos, and B. A. White
Differential geometric guidance based on the involute of the target's trajectory
J. Guid., Control, Dyn., vol. 28, no. 5, pp. 990–996, 2005.
- [18] R. Tsalik and T. Shima
Circular impact-time guidance
J. Guid., Control, Dyn., vol. 42, no. 8, pp. 1836–1847, 2019.
- [19] R. Tekin, K. S. Erer, and F. Holzapfel
Polynomial shaping of the look angle for impact-time control
J. Guid., Control, Dyn., vol. 40, no. 10, pp. 2668–2673, 2017.
- [20] R. Tekin, K. S. Erer, and F. Holzapfel
Adaptive impact time control via look-angle shaping under varying velocity
J. Guid., Control, Dyn., vol. 40, no. 12, pp. 3247–3255, 2017.
- [21] R. Tekin, K. S. Erer, and F. Holzapfel
Impact time control with generalized-polynomial range formulation
J. Guid., Control, Dyn., vol. 41, no. 5, pp. 1190–1195, 2018.
- [22] S. He, W. Wang, D. Lin, and H. Lei
Consensus-based two-stage salvo attack guidance
IEEE Trans. Aerosp. Electron. Syst., vol. 54, no. 3, pp. 1555–1566, Jun. 2018.
- [23] P. Wang, Y. Guo, G. Ma, and B. Wie
New differential geometric guidance strategies for impact-time control problem
J. Guid., Control, Dyn., vol. 42, no. 9, pp. 1982–1992, 2019.
- [24] J. Lee, I. Jeon, and M. Tahk
Guidance law to control impact time and angle
IEEE Trans. Aerosp. Electron. Syst., vol. 43, no. 1, pp. 301–310, Jan. 2007.
- [25] S. Kang and H. J. Kim
Differential game missile guidance with impact angle and time constraints
IFAC Proc. Vol., vol. 44, no. 1, pp. 3920–3925, 2011.
- [26] S. Arita and S. Ueno
Optimal feedback guidance for nonlinear missile model with impact time and angle constraints
in *Proc. AIAA Guid., Navigat., Control Conf.*, 2013, Paper AIAA 2013–4785.
- [27] T. Kim, C. Lee, I. Jeon, and M. Tahk
Augmented polynomial guidance with impact time and angle constraints
IEEE Trans. Aerosp. Electron. Syst., vol. 49, no. 4, pp. 2806–2817, Oct. 2013.
- [28] R. Livermore, R. Tsalik, and T. Shima
Elliptic Guidance
J. Guid. Control Dyn., vol. 41, no. 11, pp. 2435–2444, 2018.
- [29] B. Jung and Y. Kim
Guidance laws for anti-ship missiles using impact angle and impact time
in *Proc. AIAA Guid., Navigat., Control Conf. Exhibit.*, 2006, Paper AIAA 2006–6432.
- [30] S. R. Kumar and D. Ghose
Sliding mode guidance for impact time and angle constraints
Proc. Inst. Mech. Eng., Part G: J. Aerosp. Eng., vol. 232, no. 16, pp. 2961–2977, 2018.
- [31] G. A. Harrison
Hybrid guidance law for approach angle and time-of-arrival control
J. Guid., Control, Dyn., vol. 35, no. 4, pp. 1104–1114, 2012.
- [32] K. S. Erer and R. Tekin
Impact time and angle control based on constrained optimal solutions
J. Guid., Control, Dyn., vol. 39, no. 10, pp. 2448–2454, 2016.
- [33] Q. Hu, T. Han, and M. Xin
New impact time and angle guidance strategy via virtual target approach
J. Guid., Control, Dyn., vol. 41, no. 8, pp. 1755–1765, 2018.
- [34] E. W. Weisstein
Circle involute
From MathWorld, 2020. [Online]. Available: <http://mathworld.wolfram.com/CircleInvolute.html>
- [35] Q. Hu, T. Han, and M. Xin
Analytical solution for nonlinear three-dimensional guidance with impact angle and field-of-view constraints
IEEE Trans. Ind. Electron., 2020, early access, doi: [10.1109/TIE.2020.2982114](https://doi.org/10.1109/TIE.2020.2982114).
- [36] S. Kang, R. Tekin, and F. Holzapfel
Generalized impact time and angle control via look-angle shaping
J. Guid. Control Dyn., vol. 42, no. 3, pp. 695–702, 2019.



Ziqi Wang received the B.S. degree in aircraft design and engineering from Northwestern Polytechnical University, Xi'an, China, in 2018. He is currently working toward the M.S. degree in control science and engineering with Beihang University, Beijing, China.

His research interests include guidance and control of aerospace vehicles, intelligent control, motion planning, and machine learning.



Qinglei Hu (Senior Member, IEEE) received the B.Eng. degree in electrical and electronic engineering from Zhengzhou University, Zhengzhou, China, in 2001, and Ph.D. degree in guidance and control from the Harbin Institute of Technology, Harbin, China, in 2006.

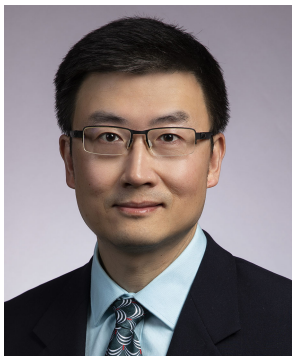
From 2003 to 2014, he had been with the Department of Control Science and Engineering with Harbin Institute of Technology and was promoted to the rank of Professor with tenure in 2012. He joined Beihang University, Beijing, China, in 2014, as a full Professor. He worked as a Post-Doctoral Research Fellow with the School of Electrical and Electronic Engineering, Nanyang Technological University, Singapore, from 2006 to 2007, and from 2008 to 2009, he visited the University of Bristol, Bristol, U.K., as a Senior Research Fellow supported by Royal Society Fellowship. After that, he visited Concordia University supported by Natural Sciences and Engineering Research Council of Canada from 2010 to 2011. His research interests include variable structure control and applications, fault-tolerant control and applications. In these areas, he has authored or co-authored over 100 technical papers.

Dr. Hu is an Associate Fellow of American Institute of Aeronautics and Astronautics (AIAA).



Tuo Han received the B.S. and M.S. degrees in guidance, navigation, and control from the Northwestern Polytechnical University, Xi'an, China, in 2014 and 2017, respectively, and is currently working toward the Ph.D. degree in control science and engineering from the Beihang University, Beijing, China.

He is currently a Visiting Researcher in aerospace with Cranfield University, Cranfield, U.K. His research interests include flight guidance and control of aerospace vehicles, and robust control theory and applications.



Ming Xin (Senior Member, IEEE) received the B.S. and M.S. degrees in automatic control from the Nanjing University of Aeronautics and Astronautics, Nanjing, China, in 1993 and 1996, respectively, and the Ph.D. degree in aerospace engineering from the Missouri University of Science and Technology, Rolla, MO, USA, in 2002.

He is currently a Professor with the Department of Mechanical and Aerospace Engineering, University of Missouri, Columbia, MO, USA. His research interests include flight mechanics, guidance, navigation, and control of aerospace vehicles, optimal control theory and applications, estimation/filtering, and cooperative control of multiagent systems.

Dr. Xin was the recipient of the U.S. National Science Foundation CAREER Award. He is an Associate Fellow of American Institute of Aeronautics and Astronautics (AIAA), a Senior Member of American Astronautical Society, and a member of American Society of Mechanical Engineers (ASME). He is an Associate Editor for *AIAA Journal of Spacecraft and Rockets* and *ASME Journal of Dynamic Systems, Measurement, and Control*, and a Technical Editor for the IEEE/ASME TRANSACTIONS ON MECHATRONICS.